KCL-PH-TH/2021-94

Probing ultra-light axions with the 21-cm Signal during Cosmic Dawn

Selim C. Hotinli,[1,*] David J. E. Marsh,[2,†] and Marc Kamionkowski[1,‡]

[1] *Department of Physics & Astronomy, Johns Hopkins University, Baltimore, MD 21218, USA*
[2] *Theortetical Particle Physics and Cosmology, King's College London, Strand, London, WC2R 2LS, United Kingdom*

(Dated: September 7, 2022)

Ultra-light axions (ULAs) are a promising and intriguing set of dark-matter candidates. We study the prospects to use forthcoming measurements of 21-cm fluctuations from cosmic dawn to probe ULAs. We focus in particular on the velocity acoustic oscillations (VAOs) in the large-scale 21-cm power spectrum, features imprinted by the long-wavelength ($k \sim 0.1\,\mathrm{Mpc}^{-1}$) modulation, by dark-matter–baryon relative velocities, of the small-scale ($k \sim 10 - 10^3\,\mathrm{Mpc}^{-1}$) power required to produce the stars that heat the neutral hydrogen. Damping of small-scale power by ULAs reduces the star-formation rate at cosmic dawn which then leads to a reduced VAO amplitude. Accounting for different assumptions for feedback and foregrounds, experiments like HERA may be sensitive to ULAs with masses up to $m_\alpha \approx 10^{-18}$eV, two decades of mass higher than current constraints.

I. INTRODUCTION

Next-generation cosmic microwave background (CMB) experiments such as the Simons Observatory (SO) [1, 2] and CMB-S4 [3], galaxy surveys such as DESI [4] and the Vera Rubin Observatory (VRO) [5], as well as 21-cm experiments such as HERA [6] or SKA1-low [7, 8] will soon generate a wealth of stringent new tests of the standard cosmological model and hopefully shed light on the nature of dark matter. Here, we consider ultra-light axions (ULAs), a dark-matter candidate that is compelling because of its possible connections to the strong-CP problem, galactic substructure, and string theory [9, 10].

Here we explore new probes of ULAs enabled by forthcoming measurements of fluctuations of the 21-cm line of neutral hydrogen during cosmic dawn. The galaxy-formation rate in any particular region of the Universe can be affected by the dark-matter–baryon relative velocity in that region. This thus introduces a fluctuation in galaxy-formation rate on the fairly large ($k \sim 0.1\,h\mathrm{Mpc}^{-1}$) coherence scale of the linear-theory dark-matter–baryon relative velocity [11]. The oscillations in the dark-matter–baryon relative-velocity power spectrum are thus imprinted in the power spectrum of 21-cm fluctuations from cosmic dawn [12–25].

ULAs (and other models of ultralight bosonic dark mater) differ from standard cold dark matter (CDM) due to their astrophysically large de Broglie wavelength, which leads to an effective sound speed in the ULA density perturbations, suppressing the growth of cosmic structure relative to CDM [9, 26, 27].[1] This effect, and other effects related to the ULA wavelength, can be probed by a wide variety of astrophysical and cosmological measurements [9, 10, 34–36]. The CMB and galaxy surveys establish a lower bound on the ULA mass around 10^{-25} eV, and probe the ULA density fraction at the percent level for lower masses [37–39]. The lower limit can be improved by a variety of cosmological probes (e.g. Refs. [40–43]), with the strongest, $m > 2 \times 10^{-20}$ eV, being provided by the Lyman-alpha forest flux power spectrum [44].

The prospects to use the 21-cm signal as probe the small-scale matter power spectrum during cosmic dawn were discussed in Ref. [24]. Here we show that the velocity acoustic oscillations (VAOs) [23] in the 21-cm power spectrum can extend the sensitivity to an ULA mass up to two orders of magnitude higher. The probe is quite robust to theoretical uncertainties as it relies on the linear-theory effects of ULAs, which are better understood than nonlinear effects. Ref. [45] showed that if the ULA Jeans scale is larger than the baryon Jeans scale, then the modulation feature in the power spectrum caused by dark-matter–baryon relative motion is absent, thus suggesting that the VAO feature would also be absent. Ref. [45] thus speculated that a future measurement of VAOs would be able to probe ULA particle masses around 10^{-18} eV. The present work addresses this claim in more detail. We compute explicitly the 21-cm cosmic dawn VAO feature from simulations and calculate the sensitivity of its amplitude to the ULA Jeans scale following Refs. [12, 20, 22, 45–47]. We forecast the sensitivity of a realistic 21-cm measurement to this effect, accounting for foreground removal and baryonic feedback.

This paper is organised as follows. We describe the 21-cm hydrogen line and relative-velocity signature in Section II. We discuss the ULAs and their effects on observables in Section III. We provide forecasts on the ULA mass in Section IV and conclude with discussion in Section V.

* shotinl1@jh.edu
† david.j.marsh@kcl.ac.uk
‡ kamion@jh.edu

[1] Note that recent studies of ULAs using N-body simulations suggest interference effects which can lead to $\sim 10-15\%$ effect on the matter power-spectrum on scales comparable to the de Broglie wavelength of the fluid (see e.g. Refs. [28–31]), which we will omit in this paper. The intereference and vorticity effects that are not captured by the fluid formulation we use here are unlikely to be significant at the power spectrum level, although a possible effect on early star formation is still an open question [32, 33].

II. THE IMPACT OF RELATIVE VELOCITIES ON THE 21-CM POWER SPECTRUM

A. The 21-cm hydrogen line

The absorption/emission of 21-cm photons by neutral hydrogen is determined by the T_s of neutral hydrogen, which can be obtained from,

$$\frac{n_1}{n_0} = \frac{g_1}{g_0} e^{-T_*/T_s}. \quad (1)$$

Here, n_0 and n_1 are the comoving number densities of the hydrogen atoms in the singlet and the triplet states, where $g_0 = 1$ and $g_1 = 3$ are their numbers of degrees of freedom, respectively. The temperature corresponding to the 21-cm hyperfine transition is $T_* = 0.068\,\mathrm{K}$. The hydrogen emits (absorbs) photons from the CMB when the local spin temperature is higher (lower) than the CMB temperature. The distribution of these photons at the different wavelengths and at different redshifts can be used to infer the astrophysical and cosmological properties of our Universe.

Our observable is the 21-cm brightness temperature [48],

$$T_{21} = 38\mathrm{mK}\left(1 - \frac{T_\gamma}{T_s}\right)\left(\frac{1+z}{20}\right)^{1/2} x_{\rm HI}(1+\delta_b)\frac{\partial_r v_r}{H(z)}\,, \quad (2)$$

where $x_{\rm HI}$ is the neutral-hydrogen fraction, $\partial_r v_r$ is the line-of-sight gradient of the velocity, T_γ is the CMB temperature, δ_b is the baryon overdensity, and H is the Hubble parameter [19, 21, 48].

We define the cosmic-dawn era to be that when the first stars formed, starting around $z \sim 25 - 35$ [49]. After recombination, the gas kinetic temperature is dominated by adiabatic cooling and the spin temperature is coupled to the CMB temperature due to the high gas density and through collisions [50]. Towards the the end of the dark ages, collisional coupling of hydrogen becomes ineffective and the 21-cm signal becomes small. The first stars produce UV photons that redshift into the Lyman-α line and couple the kinetic and spin temperatures of hydrogen in the intergalactic medium (IGM) via the Wouthuysen-Field effect [51–53]. Remnants of these first stars likely produce a background of $\sim 0.1 - 2$ keV X-rays [54, 55] heating the IGM before reionization progresses largely after $z \sim 10$ [56–58]. Toward the end of reionization ($z \lesssim 10$), Lyman-Werner feedback reduces the effects of streaming velocities in the IGM on the 21-cm signal[49, 59].

We model the 21-cm fluctuations during cosmic-dawn with semi-numerical simulations provided by `21cmvFAST`[2], which is built upon `21cmFAST`[3]. Initial conditions for peculiar velocity and density fields are set at $z = 300$ with a Gaussian random field in Lagrangian space, before being evolved with the Zel'dovich approximation [60] to match the mean collapse fraction for the conditional Sheth-Tormen halo mass function [61]. The photon emission rates of the sources embedded in each halo are assumed proportional to the increase of the total collapsed halo mass. The excursion set formalism is used in each cell to estimate the mean number of sources contributing to the gas temperature from the surroundings. The kinetic temperature is calculated including adiabatic expansion, Compton scattering with the CMB [62], and the inhomogeneous heating history of the IGM (please see for details on this calculation in Refs. [63, 64]).

For each observed frequency, we produce realizations of the 21-cm signal of coeval cubes of size 2000 Mpc on 2000^3 grids. Each coeval cube is simulated at the respective redshift from an initial density field given by appropriate transfer functions for relative velocities and matter. The power spectrum $\Delta^2_{21}(k)$ of 21-cm fluctuations satisfy

$$\langle \delta T_{21}(\vec{k}, z)\delta T^*_{21}(\vec{k}', z)\rangle = (2\pi)^3\delta(\vec{k} - \vec{k}')\frac{2\pi^2}{k^3}\Delta^2_{21}(k, z)\,, \quad (3)$$

where $\delta T_{21}(\vec{k}, z)$ is the Fourier transform of $[T_{21}(\vec{x}) - \bar{T}_{21}]/\bar{T}_{21}$, the zero-mean fluctuations of the 21-cm brightness temperature at redshift z.

B. The impact of relative velocities

The modulation induced by the dark-matter–baryon relative velocities on the 21-cm power spectrum can be captured from the statistics of the collapsed baryonic

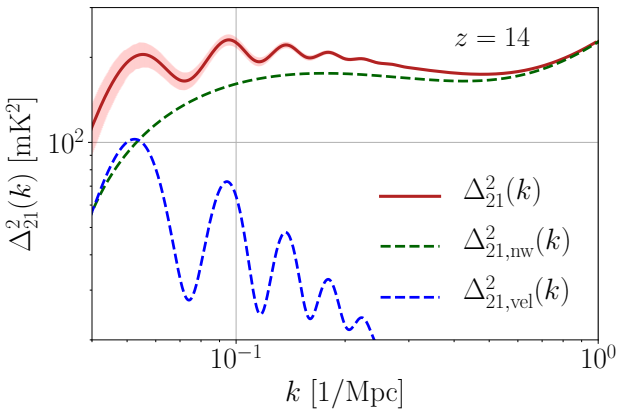

FIG. 1. The brightness-temperature power spectra of t he 21-cm hydrogen line at redshift $z = 14$ (in solid red), shown with fitted contribution to the power spectra (in dashed green) in the absence of the relative velocity effect and the velocity contribution (dashed blue) as discussed in Section II B. For the simulations we used `21cmvFAST` [23] with medium feedback. Error bars shown in the figure for the signal are Poisson errors from our simulations. The dashed green line is a fourth-order polynomial fit, as discussed in Section II B.

[2] github.com/JulianBMunoz/21cmvFAST
[3] github.com/andreimesinger/21cmFAST

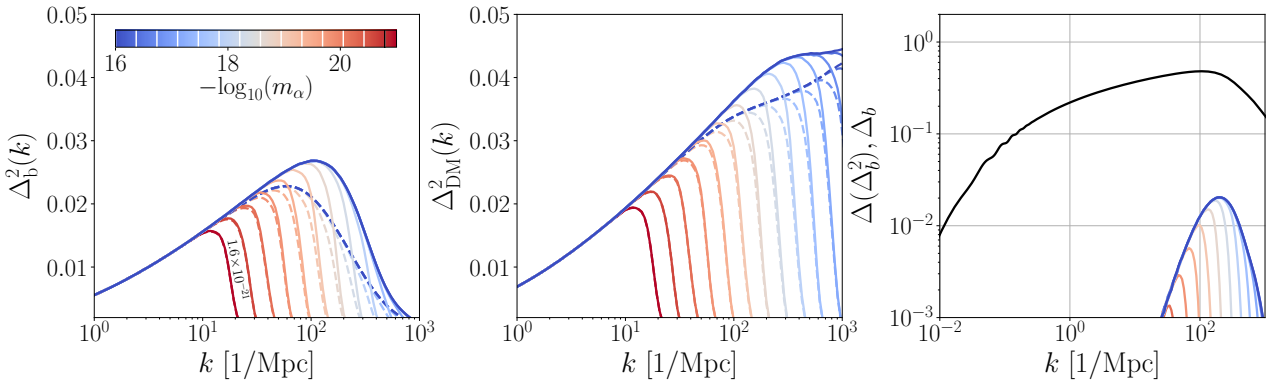

FIG. 2. **The effect of ULAs on the baryon and DM power-spectra.** *The left and middle plots* show the baryon and dark matter power-spectra for varying ULA mass, respectively. The ULAs can be observed to dampen the structure formation on small scales. Here, the solid (dashed) colored lines correspond to the power spectra in the absence (presence) of the relative velocity effect as shown in e.g. Refs. [12, 20, 46, 47]. *The right plot* compares the characteristic baryon overdensity $\Delta_b(k) = [\int_0^k k'^3 \mathrm{d}k'/(2\pi^2) P_b(k')]^{1/2}$ (solid black line) in the absence of ULAs with the characteristic change in the small-scale baryon power about their mean value $\Delta(\Delta_b^2) \equiv |\Delta_b^2(k, v_{\rm cb} = 0) - \Delta_b^2(k, v_{\rm cb})|$ (colored lines) as function of wavenumber k. The amplitude of the quadratic small-scale fluctuations ($k \sim 100 h\mathrm{Mpc}^{-1}$) shown as comparable with the linear power-spectra on large scales ($k \sim 0.01 h\mathrm{Mpc}^{-2}$). *On all plots*, different colors correspond to the scenarios with ULAs with varying mass at redshift $z = 20$. The masses are highlighted with white markers on the colorbar shown on the left panel. The right-most line (highlighted with the black marker on the colorbar) corresponds to $m_\alpha = 1.6 \times 10^{-21}$eV, with succeeding lines to the left corresponding to masses as highlighted on the colorbar.

density to a good approximation. Briefly, the effect of bulk relative velocities is analogous to that of the gas pressure, which suppresses the accretion of baryons. The bulk kinetic energy of the gas gets converted into thermal energy as it falls into the dark matter (DM) halo, resulting in a change in the effective sound speed $c_{\rm eff,s} \simeq (c_s^2 + v_{\rm cb}^2)^{1/2}$, hence in the baryon collapsed fraction [12–19, 21, 22, 65]. The effect of the relative velocities on the 21-cm brightness temperature power spectrum amplitude can then be parameterised as [23]

$$\Delta^2_{21,\rm vel}(k,z) = A_{\rm vel}(z)\Delta^2_{v^2}(k,z)|W(k,z)|^2\,, \qquad (4)$$

where $A_{\rm vel}$ is some redshift-dependent amplitude of fluctuations. The window function $W(k,z)$ depends on the various contributors to the 21-cm power spectrum such as Lyman-α coupling and X-ray heating. Here, we defined $\Delta^2_{v^2}(k)$ as the power spectrum of the quantity

$$\delta_{v^2} = \sqrt{\frac{3}{2}}\left(\frac{v_{\rm cb}^2}{v_{\rm rms}^2} - 1\right)\,, \qquad (5)$$

which accurately captures the shape of the effect of relative velocities on the observables for the scales where the 'streaming' bulk relative velocity can be approximated with a root-mean-squared value $v_{\rm rms} \simeq 30\,\mathrm{km\,s^{-1}}$ at recombination [11]. As the VAOs are statistically independent from the density fluctuations at first order, the amplitude of the 21-cm power spectrum can be written as

$$\Delta^2_{21}(k,z) = \Delta^2_{21,\rm vel}(k,z) + \Delta^2_{21,\rm nw}(k,z)\,, \qquad (6)$$

where $\Delta^2_{21,\rm nw}(k,z)$ is the component *excluding* VAOs. Throughout this paper we use a fourth-order polynomial to parametrise the smooth contribution to the spectra following Ref. [22],

$$\ln[\Delta^2_{21,\rm nw}(k,z)] = \sum_{i=0}^{4} c_i(z)[\ln k]^i\,, \qquad (7)$$

where $c_i(z)$ are coefficients we fit for using simulations we discussed above. The fitted smooth spectra serve as our phenomenological model that captures the dependence of the 21-cm power spectra to the cosmological parameters. In what follows we marginalise over these coefficients in our forecasts. We model the power spectrum of the velocity as in Ref. [23] using the form we defined in Eq. (4). We use `21cmvFAST` to calculate the window function and the amplitude $A_{\rm vel}(z)$ for a given feedback model, and calculate $\Delta^2_{v^2}$ for a given cosmology. We calculate the relative-velocity transfer function at the end of recombination using `CLASS` Boltzmann solver [66], which we use as an initial condition for our simulations. We show the effect of relative velocities on the 21-cm power spectrum at redshift $z = 14$ in Fig. 1 for the medium baryonic feedback scenario defined in `21cmFAST`.

III. ULAS AND THEIR EFFECTS ON OBSERVABLES

A. ULA equations of motion and the density power-spectra

A coherently oscillating scalar field ϕ in a quadratic potential $V = m_\alpha^2\phi^2/2$ has an energy density that scales as a^{-3} and thus can behave in cosmology as DM [67].

The Klein-Gordon equation is

$$(\Box - m_\alpha^2)\phi = 0\,, \tag{8}$$

where $\Box$ is the D'Alembertian for the cosmological spacetime, and m_α is the axion mass. At zeroth order in cosmological perturbation theory, the solution of this equation for the field initially displaced a fixed amount from the vacuum leads to production of the ULA DM relic density via realignment [67–70]. At higher orders in perturbation theory, the ULA field is coupled to the gravitational potential, and undergoes structure formation. The difference between ULAs and CDM arises due to the gradient terms in $\Box$, which in linear perturbation theory lead to a sound speed in the effective ULA fluid equations [26, 71–73].

In the moving background of the DM-baryon relative velocity the ULA and baryon fluid equations are [45]

$$\dot{\delta}_\alpha = \frac{i\mu}{a}\,\delta_\alpha - \theta_\alpha\,, \tag{9}$$

$$\dot{\theta}_\alpha = \frac{i\mu}{a}\,\theta_\alpha - \frac{3}{2}H^2[\Omega_\alpha(t)\delta_\alpha + \Omega_b(t)\delta_b] - 2H\theta_\alpha + \frac{k^2 c_{s,a}^2}{a^2}\delta_\alpha\,, \tag{10}$$

$$\dot{\delta}_b = -\theta_b\,, \tag{11}$$

$$\dot{\theta}_b = -\frac{3}{2}H^2[\Omega_\alpha(t)\delta_\alpha + \Omega_b(t)\delta_b] - 2H\theta_b + \frac{c_{s,b}^2 k^2}{a^2}(\delta_b + \delta_T)\,, \tag{12}$$

$$\dot{\delta}_T = \frac{2}{3}\dot{\delta}_b + \frac{T_\gamma}{T_g}\frac{\Gamma_C}{H(1+z)}\delta_T, \tag{13}$$

where $\mu = \vec{v}_{b\alpha}^{\,(\mathrm{bg})}(t)\cdot\vec{k}$, Ω_α is the ULA density, Ω_b is the baryon density, $\vec{v}_{b\alpha}^{\,(\mathrm{bg})}$ is the ULA-baryon relative velocity, $c_{s,b}$ is the baryon sound-speed, and $c_{s,a}$ is the ULA sound-speed, Γ_C is Compton interaction rate, T_γ is the CMB temperature, T_g is the gas temperature and we include the effect of temperature fluctuations $\delta_T = \delta_{T_g}/T_g$. On sub-horizon scales, the ULA sound speed is approximated as

$$c_{s,\alpha}^2 \approx \frac{k^2}{4m_\alpha^2 a^2}\,. \tag{14}$$

We solve these equations given the initial conditions for a ΛCDM Universe at matter-radiation equality that we compute using CLASS [66]. The ULA sound speed leads to a suppression of power relative CDM (which has $c_s = 0$). Using CDM initial conditions is not exactly accurate for ULAs, since there is already some departure from CDM at high redshift in the transfer function (see e.g. Refs. [37, 72]), however the dynamical suppression of structure for $z < 1010$ caused by the sound speed gives an accurate model at low z (such an approach was taken in Refs. [74, 75]).

We demonstrate this suppression in clustering statistics with the power-spectra of the baryon and matter fluctuations in Fig. 2. In these figures we also show the suppression in clustering due to DM-baryon relative-velocity which increases the baryon pressure experienced by halos. While on large scales ($k \sim 0.1\mathrm{Mpc}^{-1}$) the fluctuations of the 21-cm temperature are enhanced due to the additional VAO term (as discussed in Sec. II B), small-scale fluctuations of density are somewhat suppressed by the relative velocities.

B. VAO amplitude

The amplitude of the VAO signature $A_{\rm vel}(z)$ depends non-linearly on the small-scale brightness temperature, which is sensitive to the baryonic feedback processes and non-linear clustering on smaller scales. Similar to Ref. [22], we can calculate the amplitude of the VAOs by defining a 21-cm relative-velocity bias in the form

$$b_{21}^2(z) = \langle T_{21}^2(v_{\rm cb})\rangle - \langle T_{21}(v_{\rm cb})\rangle^2 \tag{15}$$

such that the relative-velocity contribution to the 21-cm power-spectra can then be written as

$$\Delta_{21,\rm vel}^2(k,z) = b_{21}^2(z)\Delta_{v^2}^2(k,z)|W(k,z)|^2\,, \tag{16}$$

and the relative-velocity bias $b_{21}(z)$ has the fiducial value of $A_{\rm vel}(z)$. In what follows, we calculate the derivative of the bias term with respect to the axion mass $\partial b_{21}^2(z)/\partial m_\alpha$ that appears in our forecasts using the analytical approximations up to quadratic order in density fluctuations as described in [20, 46, 47]. We set the fiducial value to $A_{\rm vel}(z)$, which we calculate from fitting Eqs. (4) and (7) to our simulations using `21cmvFAST` with no ULAs (equivalent to $m_\alpha \to \infty$). We demonstrate the effect of ULAs on the 21-cm power-spectra in Fig. 3 which lead a suppression of the quadratic contribution to the VAO amplitude. As shown in Ref. [20], because the VAO signature in the 21-cm temperature fluctuations is inherently quadratic, the VAO signature in the 21-cm temperature *power-spectrum* amplitude $\Delta_{21,\rm vel}^2(k)$, at wavenumber k, ends up being sensitive to smaller scales than k. This allows the VAO signature to be sensitive to small scales where ULAs suppressed the density fluctuations. ULAs cut-off the power spectrum on small scales, and remove the (higher order) modulating effect of the DM-baryon relative velocity on the small scale matter power spectrum. Thus, a cut-off in the power spectrum on k smaller than the baryon smoothing scale drastically reduces the quadratic contribution to the VAO amplitude, as anticipated in Ref. [45]. This is the primary physical effect demonstrated explicitly for the first time in the present work (Fig. 3), and drives the forecasted constraints that follow.

Note that the 21-cm temperature-brightness signal at redshift $z \sim$16 corresponds to the halfway point throughout the heating transition marked by large fluctuations compared to the later times ($z \sim$14) where X-rays heat up the IGM, making the power-spectrum (and the VAO signature) smaller and less pronounced, as well as earlier times where Lyman-α becomes comparable to the X-ray,

as demonstrated by the redshift evolution of the signal visible in Fig. 3.

In a nut-shell, the VAO feature on large scales (the velocity coherence scale) are induced by the second order modulation of the power spectrum by relative velocity on small scales (near the baryon Jeans scale). The amplitude and shape of the VAO decouple, and the amplitude can be estimated by computing the velocity bias, $b_{21}(z)$, in moving background perturbation theory. ULAs damp the power on scales below the axion Jeans scale. Thus, if the axion Jeans scale is larger than the baryon Jeans scale, relative velocities induce no power spectrum modulation in moving background pertrubation theory [45], the velocity bias vanishes, and thus too do the large scale VAO.

The analytic approximation to $b_{21}(z)$ has been shown to match the qualitative features of the relative-velocity contribution to the power-spectra while also predicting $A_{\rm vel}(z)$ to be an $\mathcal{O}(1)$ lower compared to more robust calculations using `21cmvFAST` simulations [22], which capture the baryonic feedback processes and the effect of non-linear structure formation more accurately. In what follows, we marginalize over the baryonic feedback strength using our simulations to account for the former, and leave evaluating the effect of non-linear structure formation on the partial derivative $\partial b_{21}^2(z)/\partial m_\alpha$ to future works. Note nevertheless that our fiducial values for $A_{\rm vel}(z)$ are robust as they are calculated from simulations.

IV. FORECASTS

A. Experimental specifications

We take four redshift bins of size $\Delta z = 2$, centred at redshifts $z \in \{12, 14, 16, 18\}$, and one redshift of size $\Delta z = 3$, centred at $z = 24$ to match Ref. [22]. These choices are made to get sufficiently high SNR per redshift bin in order to detect the VAO features using experimental specifications matching HERA survey [6].

Foreground mitigation for the cosmological 21-cm signal is performed either via wedge suppression or avoidance[4]. `21cmSense` [78–80] is a python module designed to estimate the noise power spectra when a given telescope array observe the 21-cm signal via foreground avoidance. We use `21cmSense` for the HERA experiment, which we describe below.

In every uv bin[5] the noise is calculated as,

$$\delta^2_{\rm uv}(\boldsymbol{k}) \approx X^2Y(\boldsymbol{k}^3/2\pi^2)(\Omega_{\rm Eff}/(2t_0))T^2_{\rm sys}, \qquad (17)$$

where X^2Y is a scalar conversion from an observed solid angle (or effective beam, $\Omega_{\rm Eff}$) to a comoving distance [81], $T_{\rm sys}$ is the system temperature, t_0 is the total observation time and $\boldsymbol{k}$ is the three-dimensional Fourier wavenumber.

Assuming Gaussian errors on cosmic variance, we express the total uncertainty with an inversely-weighted sum across all the k modes as

$$\Delta^{2,\rm obs}_{21}(k) = \left\{ \sum_i \frac{1}{[\delta^2_{{\rm uv},i}(k) + \Delta^2_{21}(k)]^2} \right\}^{-\frac{1}{2}}, \qquad (18)$$

where the index, i, represents multiple measurements of the same frequency from redundant baselines within the array. This is therefore the total noise, including both sample variance and thermal noise.

The foreground wedge is defined as

$$k_\parallel = a + bk_\perp\,, \qquad (19)$$

where $k_\parallel$ and $k_\perp$ are the Fourier modes projected on the line-of-side and the transverse plane respectively; b depends on the instrument beam, bandwidth and underlying cosmology; a is the buffer zone, typically chosen as $a = 0.1h{\rm Mpc}^{-1}$ ($a = 0.01h{\rm Mpc}^{-1}$) for pessimistic (optimistic) scenarios.

We apply `21cmSense` to HERA [82, 83], where stations are located in a filled hexagonal grid (11 along each side). Each station is 14 m in diameter giving a total collecting area of 50,953 m^2 accross a total bandwidth ranging $[50, 250]$ MHz. The antennae are taken to be at $T_{\rm rx} = 100$K. HERA is operated only in drift scan mode for 6 hours per night. Throughout the paper we assume three years of observation with HERA.

For reference, we calculate the total SNR as equal to $\sum_k \Delta^2_{21}(k,z)/\Delta^{2,\rm obs}_{21}(k,z)$ and the VAO SNR as equal to $\sum_k \Delta^2_{21,\rm vel}(k,z)/\Delta^{2,\rm obs}_{21}(k,z)$, summed (in quadrature) over the redshift bins we consider. Here, $\sum_k$ is the sum over binned wavenumbers and $\Delta^{2,\rm obs}_{21}(k,z)$ is the total uncertainly of the 21-cm spectra defined in Eq. (13). We set the k-bin widths to the inverse of the cosmological bandwidth corresponding to the redshift range that can be considered co-eval as in [6]. We find the total (over all z) detection signal-to-noise ratio (SNR) of the 21-cm signal to be $\{130, 190, 498\}$, and the SNR of the VAO signature to be $\{21, 40, 190\}$, for our $\{\text{pessimistic}, \text{moderate}, \text{optimistic}\}$ foreground considerations, respectively, and for regular baryonic feedback, using HERA [6].

B. Results

We define the information matrix as

$$F_{\alpha\beta}(z) = \sum_{k-\rm bins} \frac{\partial_\alpha \Delta^2_{21}(k,z)\partial_\beta \Delta^2_{21}(k,z)}{(\Delta^2_{21,\rm obs})^2(k,z)}\,, \qquad (20)$$

[4] Please see [76, 77] for detailed description of the EoR window and foreground wedge.

[5] The uv plane is the Fourier transform of the sky brightness distribution in a plane perpendicular to the direction of observation. Radio interferometers cannot produce an image of the sky directly, instead they make observations in the uv plane.

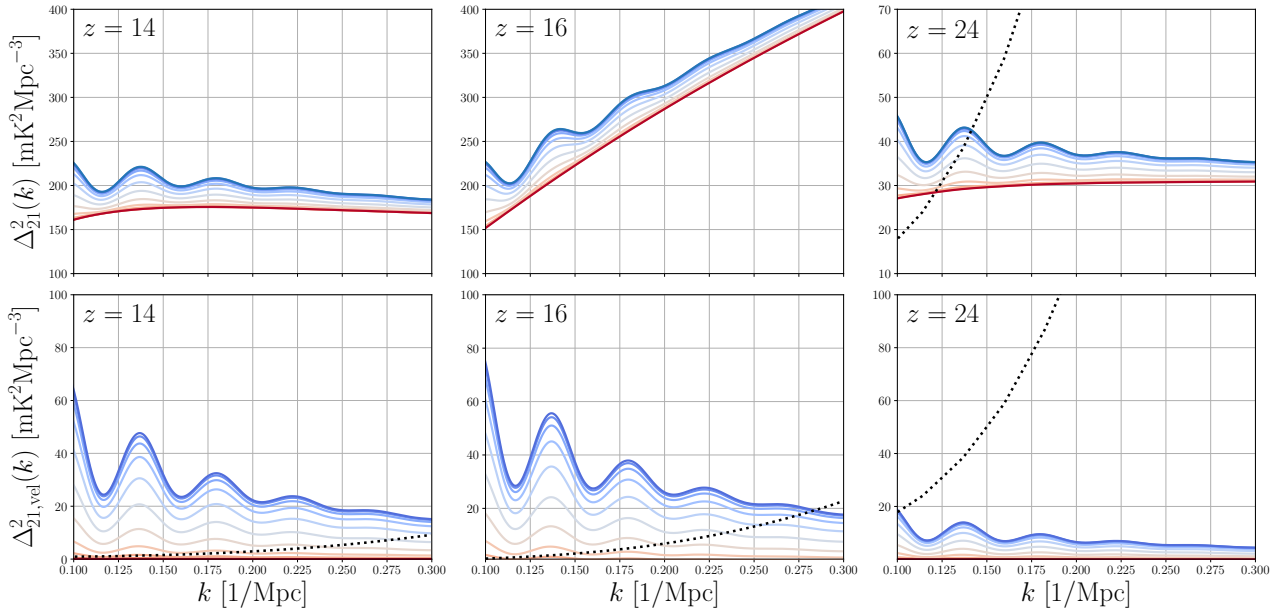

FIG. 3. **The effect of ULAs on the VAO signature in the 21-cm power-spectra for redshift bins centred at $z = \{14, 16, 24\}$**. The VAO amplitude can be shown to vary with m_α. The dotted black lines correspond to the anticipated noise (cosmic variance and thermal noise combined) for the HERA experiment, which we calculate with `21cmSense`. We discuss the binning in wavenumber k in Sec. IV. Upper plots correspond the 21-cm signal. The blue end of the color spectrum corresponds to the prediction from the ΛCDM cosmology, averaged over 20 simulations with `21cmvFAST`. We demonstrate the effect of ULAs on the 21-cm power spectrum with varying colors. See Fig. 2 for the correspondence between different colors and the ULA mass. Here, the effect of ULAs are calculated analytically using Refs. [20, 46, 47] as discussed in Sec. III B.

and model the 21-cm power-spectra with

$$\{c_0(z), c_1(z), c_2(z), c_3(z), c_4(z), m_\alpha, \epsilon_{\rm FB}(z)\}\,, \quad (21)$$

at each redshift bin we consider, where $c_i(z)$ with $i \in \{0, \ldots, 4\}$ parametrises the non-wiggle part of the 21-cm power-spectra, m_α is the ULA mass, and $\epsilon_{\rm FB}$ is a parameter representing the sensitivity of the 21-cm power-spectra to the Lyman-Werner (LW) baryonic feedback efficiency in the `21cmFAST` simulations we consider, which parametrise the formation of stars as a change of mass of cooling haloes as [84, 85]

$$M_{\rm cool}(z, v_{\rm cb}, F_{\rm LW}) = M_{\rm cool}(z, v_{\rm cb}, 0) \times [1 + \epsilon_{\rm FB} B(F_{\rm LW})^\beta]\,, \quad (22)$$

where $M_{\rm cool}(z, v_{\rm cb}, 0)$ is the mass of cooling in the absence of LW feedback, $F_{\rm LW} = 1.256 \times 10^{-20}$ergs s^{-1}cm^{-2}Hz^{-1}sr^{-1} is the LW flux, $B = 4$ and $\beta = 0.47$ as fitted to the simulations in Refs. [86, 87].

In Fig. 4, we show the total signal-to-noise (SNR) on the ULA mass from the five redshift bins defined above. The colored vertical lines indicate that ULA masses lower than $m_\alpha = 6.0 \times 10^{-19}$ eV will be detected with an SNR of 5 or higher. The dotted black horizontal line correspond to SNR of 5. The SNR goes to zero for high ULA mass where the effect of the ULA on the 21-cm is negligible. The SNR flattens at low masses where models with different ULA masses cannot be distinguished from each other. Here, the buffer zone is set as $a = 0.05h$Mpc^{-1}, corresponding to our *moderate* foreground scenario we describe next.

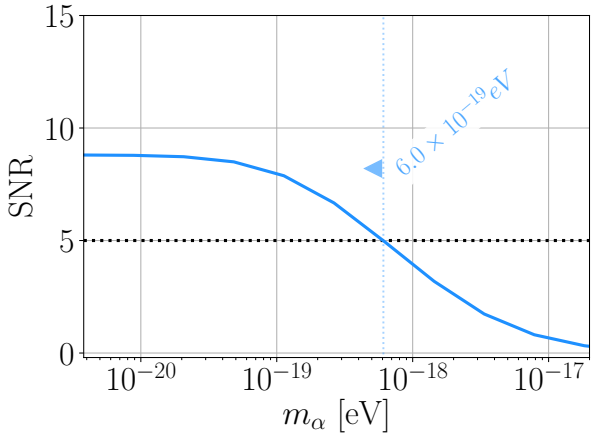

FIG. 4. The total SNR on the ULA mass using foreground cut-off scale $a = 0.05h$Mpc^{-1}, assuming moderate baryonic feedback and HERA survey specifications as we describe in the text. The SNR of the ULA mass detection is plotted for varying ULA mass m_α. The vertical lines indicate that ULA masses lower than $m_\alpha = 6.0 \times 10^{-19}$ eV will be detected with an SNR of 5 or higher. The horizontal lines correspond to SNR of 3. The SNR goes to zero for high ULA masses and flattens at low masses where scenarios with different ULA masses cannot be distinguished from each other.

Foregrounds play an important role in determining our ability to infer cosmology from the 21-cm signal. We demonstrate how various foreground scenarios affect the constraints on the ULA mass in Fig. 5. Here, we have

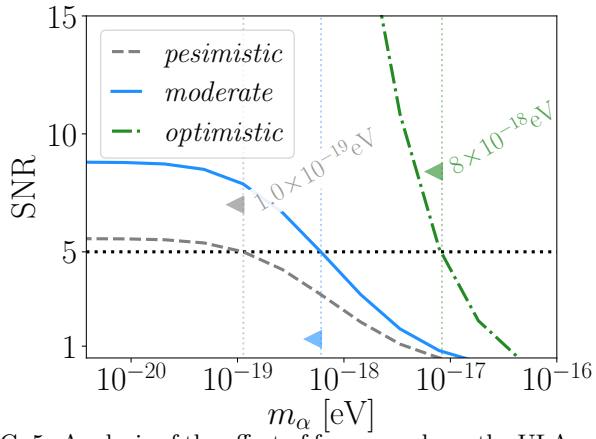

FIG. 5. Analysis of the effect of foregrounds on the ULA mass constraints. Three foreground scenarios are shown, these are *pessimistic* (dashed grey line), moderate (solid blue line) and *optimistic* (dot-dashed green line). The upper limits on the ULA mass can be seen to worsen for the *pessimistic* foreground scenario where masses below 1.0×10^{-19}eV are constrained with SNR > 5. For the *optimistic* scenario, ULA masses below 8.0×10^{-18} eV are constrained with SNR above 5. The *moderate* scenario is identical to the results shown if Fig. 4.

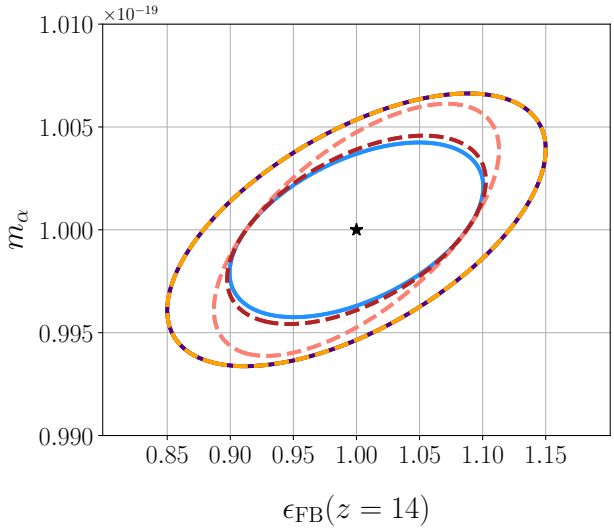

Description of the observables	Color
$z_{\rm bin} \in \{14\}$	Indigo
$z_{\rm bin} \in \{14, 24\}$	Orange
$z_{\rm bin} \in \{14, 18, 24\}$	Salmon
$z_{\rm bin} \in \{14, 16, 18, 24\}$	Brown
$z_{\rm bin} \in \{12, 14, 16, 18, 24\}$	Blue

FIG. 6. Contour plots demonstrating the improvement on the ULA mass constraints from the redshift information, for fiducial values of $m_\alpha = 10^{-19}$eV and $\epsilon_{\rm FB} = 1$. The foremost contour (solid, indigo colour) corresponds to the constraints from a single redshift bin centered at $z = 14$. Following dashed contours correspond to successively adding information from redshift bins centered at $z = \{24, 18, 16, 12\}$ with colors described above. Innermost plot correspond to adding all redshift bins, matching our *moderate* foreground scenario (shown with blue solid contour) forecasts described before. The redshift information can be seen to improve the ULA mass estimate along the degeneracy direction. We find the VAO measurements can potentially measure the axion mass of $m_\alpha = 10^{-19}$eV over 95% precision.

defined the scenario where the baselines are added incoherently, no k modes are included from within the horizon wedge (and buffer zone) and $a = 0.1h$Mpc^{-1} as *pessimistic*. In the *moderate* scenario, the baselines are added coherently and a =$0.05h$Mpc^{-1}, otherwise same as the *pessimistic* scenario. In the *optimistic* scenario, all baselines in the primary field of view (no buffer zone) are added coherently and a =$0.03h$Mpc^{-1}. We find ULA masses below 1.0×10^{-19} eV and 8×10^{-18} eV will be detected to SNR of 3 or higher for the pessimistic and optimistic scenarios, respectively. The SNR exceeds 10 by $m_\alpha = 10^{-18}$ eV in the optimistic scenario, while flattening around ~ 5 in the pessimistic scenario.

Another important factor when detecting the ULAs is the effect of baryonic feedback, which suppresses the VAO signature [22]. Moreover, if feedback affects the 21-cm in a similar way, we might expect the ULA mass to be somewhat degenerate with $\epsilon_{\rm FB}$. Indeed in Fig. 6 we show that for a single redshift bin, the effect of baryonic feedback has some degeneracy with m_α. Here, we show the $m_\alpha - \epsilon_{\rm FB}$ contour plots from various combinations of the redshift bins. The foremost solid contour in indigo corresponds to the constraints from the redshift bin centered at $z = 14$. Following dashed contours corresponds to successively adding information from redshift bins centered at $z = \{24, 18, 16, 12\}$, with colors described in the figure caption. Innermost blue solid contour correspond to the forecasts from adding all redshift bins, matching our *moderate* foreground scenario. The redshift information can be seen to improve the ULA mass estimate along the degeneracy direction suggesting the degeneracy between the ULA mass and the feedback parameter $\epsilon_{\rm FB}$ at $z = 14$ is somewhat broken.

Lastly, we expect our forecasts to depend on assumptions about baryonic feedback, which affects the large-scale 21-cm spectrum by preventing smaller-mass molecular-cooling haloes to form stars, in turn the reducing the effect of relative-velocities on the 21-cm fluctuations. In Fig. 7, we show the ULA mass constraints for different feedback models defined in `21cmFAST`. Indeed, lower (higher) feedback levels lead to more optimistic (pessimistic) constraints.

V. DISCUSSION AND CONCLUSIONS

Ultra-light axions (ULAs) are a well-motivated candidate to compose all or some of the dark matter and can have a wide range of particle masses. The velocity acoustic oscillation (VAO) signature in the 21-cm spectrum on large scales provides a window to test ULAs through its sensitivity to small-scale fluctuations in gas density and

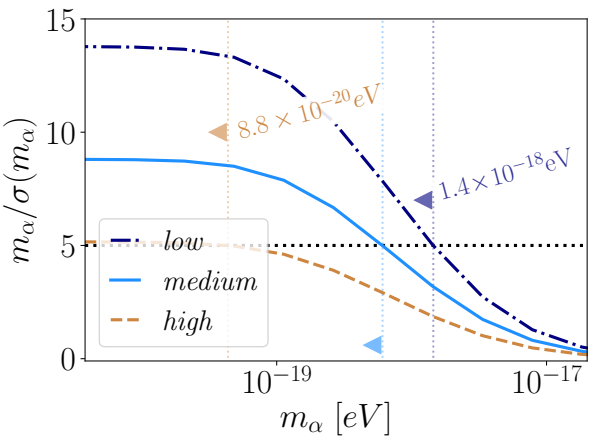

FIG. 7. Analysis of baryonic feedback assuming three feedback levels as defined in `21cmFAST`. Higher baryonic feedback strength prevents the forming of smaller-mass halos reducing the effect of relative-velocities on the 21-cm spectra on large scales. The blue solid line correspond to the *medium* feedback scenario assumed throughout the rest of this paper. Dot-dashed dark blue (dashed brown) line correspond to *low* (*high*) feedback scenario. Similar to before, we show the 3 sigma constraints on the ULA mass with vertical lines matching the different lines in color.

temperature. This signal is most pronounced during the cosmic dawn era ($z \sim 10-30$) where the typical mass of collapsed baryonic objects falls near the critical mass below which gas pressure prevents their collapse.

We have evaluated the detection prospects of ULAs with measurements of the 21-cm fluctuations from cosmic dawn. The ongoing HERA experiment may be able to constrain ULA mass below 6.0×10^{-19} eV at SNR of 5 for moderate foreground and feedback scenarios. The sensitivity weakens by a factor ~ 4 if the foregrounds end up more detrimental or by ~ 3 if the baryonic feedback strength is larger. Conversely, if the foregrounds are lower, the sensitivity can be higher by a factor of ~ 5. Similarly, lower baryonic feedback can also improve the ULA sensitivity by a factor of ~ 2. Improvements such as this bridge the gap between large scale existing cosmological bounds, and small-scale constraints from galaxy evolution and black-hole physics [88–90], closing the gaps in ULA parameter space [91].

Much is yet unknown about the astrophysics of the cosmic dawn era. In particular, our ability to detect the VAO signature to high significance to infer cosmology depends on the baryonic feedback strength and the severity of foreground contamination. Here, we have shown how these complications affect constraints to ULAs using a simple information-matrix analysis and assuming phenomenological parameters represent the underlying cosmology and astrophysics. Going forward, we could build upon the observations made in this paper by more rigorous simulations with wider-ranging assumptions and modelling to test our predictions. Nevertheless, we foresee a bright future for the cosmological significance of the cosmic-dawn signal, and its potential role in constraining ULA mass.

VI. ACKNOWLEDGEMENTS

SCH thanks T. Binnie and J. B. Muñoz for useful conversations. SCH is supported by the Horizon Fellowship from Johns Hopkins University. DJEM is supported by an Ernest Rutherford Fellowship from the Science and Technologies Facilities council of the United Kingdom. This work was performed in part at Aspen Center for Physics, which is supported by National Science Foundation grant PHY-1607611, and a grant from the Simons Foundation. This work was supported at JHU in part by the Simons Foundation and by National Science Foundation grant No. 2112699.

[1] James Aguirre *et al.* (Simons Observatory), "The Simons Observatory: Science goals and forecasts," (2018), arXiv:1808.07445 [astro-ph.CO].

[2] Adrian Lee, Maximilian H. Abitbol, Shunsuke Adachi, Peter Ade, James Aguirre, Zeeshan Ahmed, Simone Aiola, Aamir Ali, David Alonso, Marcelo A. Alvarez, and et al., "The Simons Observatory," in *Bulletin of the American Astronomical Society*, Vol. 51 (2019) p. 147, arXiv:1907.08284 [astro-ph.IM].

[3] Kevork N. Abazajian *et al.* (CMB-S4), "CMB-S4 Science Book, First Edition," (2016), arXiv:1610.02743 [astro-ph.CO].

[4] Amir Aghamousa *et al.* (DESI), "The DESI Experiment Part I: Science,Targeting, and Survey Design," (2016), arXiv:1611.00036 [astro-ph.IM].

[5] LSST Science Collaboration, P. A. Abell, J. Allison, S. F. Anderson, J. R. Andrew, J. R. P. Angel, L. Armus, D. Arnett, S. J. Asztalos, T. S. Axelrod, and et al., "LSST Science Book, Version 2.0," ArXiv e-prints (2009), arXiv:0912.0201 [astro-ph.IM].

[6] David R. DeBoer *et al.*, "Hydrogen Epoch of Reionization Array (HERA)," Publ. Astron. Soc. Pac. **129**, 045001 (2017), arXiv:1606.07473 [astro-ph.IM].

[7] Robert Braun, Anna Bonaldi, Tyler Bourke, Evan Keane, and Jeff Wagg, "Anticipated Performance of the Square Kilometre Array – Phase 1 (SKA1)," arXiv e-prints , arXiv:1912.12699 (2019), arXiv:1912.12699 [astro-ph.IM].

[8] David J. Bacon *et al.* (SKA), "Cosmology with Phase 1 of the Square Kilometre Array: Red Book 2018: Technical specifications and performance forecasts," Publ. Astron. Soc. Austral. **37**, e007 (2020), arXiv:1811.02743 [astro-ph.CO].

[9] Asimina Arvanitaki, Savas Dimopoulos, Sergei Dubovsky, Nemanja Kaloper, and John March-Russell, "String Axiverse," Phys. Rev. D **81**, 123530 (2010), arXiv:0905.4720 [hep-th].

[10] David J. E. Marsh, "Axion Cosmology," Phys. Rept. **643**, 1–79 (2016), arXiv:1510.07633 [astro-ph.CO].

[11] Dmitriy Tseliakhovich and Christopher Hirata, "Relative velocity of dark matter and baryonic fluids and the formation of the first structures," Phys. Rev. **D82**, 083520 (2010), arXiv:1005.2416 [astro-ph.CO].

[12] Neal Dalal, Ue-Li Pen, and Uros Seljak, "Large-scale BAO signatures of the smallest galaxies," JCAP **1011**, 007 (2010), arXiv:1009.4704 [astro-ph.CO].

[13] Smadar Naoz, Naoki Yoshida, and Nickolay Y. Gnedin, "Simulations of Early Baryonic Structure Formation with Stream Velocity: I. Halo Abundance," Astrophys. J. **747**, 128 (2012), arXiv:1108.5176 [astro-ph.CO].

[14] Thomas Greif, Simon White, Ralf Klessen, and Volker Springel, "The Delay of Population III Star Formation by Supersonic Streaming Velocities," Astrophys. J. **736**, 147 (2011), arXiv:1101.5493 [astro-ph.CO].

[15] Matthew McQuinn and Ryan M. O'Leary, "The impact of the supersonic baryon-dark matter velocity difference on the $z \sim 20$ 21cm background," Astrophys. J. **760**, 3 (2012), arXiv:1204.1345 [astro-ph.CO].

[16] Athena Stacy, Volker Bromm, and Abraham Loeb, "Effect of Streaming Motion of Baryons Relative to Dark Matter on the Formation of the First Stars," Astrophys. J. **730**, L1 (2011), arXiv:1011.4512 [astro-ph.CO].

[17] Anastasia Fialkov, Rennan Barkana, Dmitriy Tseliakhovich, and Christopher M. Hirata, "Impact of the Relative Motion between the Dark Matter and Baryons on the First Stars," Mon. Not. Roy. Astron. Soc. **424**, 1335–1345 (2012), arXiv:1110.2111 [astro-ph.CO].

[18] Jaiyul Yoo, Neal Dalal, and Uros Seljak, "Supersonic Relative Velocity Effect on the Baryonic Acoustic Oscillation Measurements," JCAP **1107**, 018 (2011), arXiv:1105.3732 [astro-ph.CO].

[19] Jonathan R. Pritchard and Abraham Loeb, "21-cm cosmology," Rept. Prog. Phys. **75**, 086901 (2012), arXiv:1109.6012 [astro-ph.CO].

[20] Yacine Ali-Haïmoud, P. Daniel Meerburg, and Sihan Yuan, "New light on 21 cm intensity fluctuations from the dark ages," Phys. Rev. D **89**, 083506 (2014), arXiv:1312.4948 [astro-ph.CO].

[21] Rennan Barkana, "The Rise of the First Stars: Supersonic Streaming, Radiative Feedback, and 21-cm Cosmology," Phys. Rept. **645**, 1–59 (2016), arXiv:1605.04357 [astro-ph.CO].

[22] Julian B. Muñoz, "Robust Velocity-induced Acoustic Oscillations at Cosmic Dawn," Phys. Rev. **D100**, 063538 (2019), arXiv:1904.07881 [astro-ph.CO].

[23] Julian B. Muñoz, "A Standard Ruler at Cosmic Dawn," Phys. Rev. Lett. **123**, 131301 (2019), arXiv:1904.07868 [astro-ph.CO].

[24] Julian B. Muñoz, Cora Dvorkin, and Francis-Yan Cyr-Racine, "Probing the Small-Scale Matter Power Spectrum with Large-Scale 21-cm Data," Phys. Rev. D **101**, 063526 (2020), arXiv:1911.11144 [astro-ph.CO].

[25] Selim C. Hotinli, Thomas Binnie, Julian B. Muñoz, Bikash R. Dinda, and Marc Kamionkowski, "Probing compensated isocurvature with the 21-cm signal during cosmic dawn," Phys. Rev. D **104**, 063536 (2021), arXiv:2106.11979 [astro-ph.CO].

[26] M. Khlopov, B. A. Malomed, and Ia. B. Zeldovich, "Gravitational instability of scalar fields and formation of primordial black holes," Mon. Not. Roy. Astron. Soc. **215**, 575–589 (1985).

[27] David J. E. Marsh and Pedro G. Ferreira, "Ultra-Light Scalar Fields and the Growth of Structure in the Universe," Phys. Rev. D **82**, 103528 (2010), arXiv:1009.3501 [hep-ph].

[28] Xinyu Li, Lam Hui, and Greg L. Bryan, "Numerical and Perturbative Computations of the Fuzzy Dark Matter Model," Phys. Rev. D **99**, 063509 (2019), arXiv:1810.01915 [astro-ph.CO].

[29] Jiajun Zhang, Hantao Liu, and Ming-Chung Chu, "Cosmological Simulation for Fuzzy Dark Matter Model," Front. Astron. Space Sci. **5**, 48 (2019), arXiv:1809.09848 [astro-ph.CO].

[30] Jan Veltmaat, Bodo Schwabe, and Jens C. Niemeyer, "Baryon-driven growth of solitonic cores in fuzzy dark matter halos," Phys. Rev. D **101**, 083518 (2020), arXiv:1911.09614 [astro-ph.CO].

[31] Bodo Schwabe and Jens C. Niemeyer, "Deep Zoom-In Simulation of a Fuzzy Dark Matter Galactic Halo," Phys. Rev. Lett. **128**, 181301 (2022), arXiv:2110.09145 [astro-ph.CO].

[32] Matteo Nori, Riccardo Murgia, Vid Iršič, Marco Baldi, and Matteo Viel, "Lyman α forest and non-linear structure characterization in Fuzzy Dark Matter cosmologies," Mon. Not. Roy. Astron. Soc. **482**, 3227–3243 (2019), arXiv:1809.09619 [astro-ph.CO].

[33] Philip Mocz *et al.*, "First star-forming structures in fuzzy cosmic filaments," Phys. Rev. Lett. **123**, 141301 (2019), arXiv:1910.01653 [astro-ph.GA].

[34] Luca Amendola and Riccardo Barbieri, "Dark matter from an ultra-light pseudo-Goldsone-boson," Phys. Lett. B **642**, 192–196 (2006), arXiv:hep-ph/0509257.

[35] Lam Hui, Jeremiah P. Ostriker, Scott Tremaine, and Edward Witten, "Ultralight scalars as cosmological dark matter," Phys. Rev. D **95**, 043541 (2017), arXiv:1610.08297 [astro-ph.CO].

[36] David J. E. Marsh and Sebastian Hoof, "Astrophysical Searches and Constraints on Ultralight Bosonic Dark Matter," (2021), arXiv:2106.08797 [hep-ph].

[37] Renée Hlozek, Daniel Grin, David J. E. Marsh, and Pedro G. Ferreira, "A search for ultralight axions using precision cosmological data," Phys. Rev. D **91**, 103512 (2015), arXiv:1410.2896 [astro-ph.CO].

[38] Renée Hlozek, David J. E. Marsh, and Daniel Grin, "Using the Full Power of the Cosmic Microwave Background to Probe Axion Dark Matter," Mon. Not. Roy. Astron. Soc. **476**, 3063–3085 (2018), arXiv:1708.05681 [astro-ph.CO].

[39] Alex Laguë, J. Richard Bond, Renée Hložek, Keir K. Rogers, David J. E. Marsh, and Daniel Grin, "Constraining Ultralight Axions with Galaxy Surveys," (2021), arXiv:2104.07802 [astro-ph.CO].

[40] Brandon Bozek, David J. E. Marsh, Joseph Silk, and Rosemary F. G. Wyse, "Galaxy UV-luminosity function and reionization constraints on axion dark matter," Mon. Not. Roy. Astron. Soc. **450**, 209–222 (2015), arXiv:1409.3544 [astro-ph.CO].

[41] Hsi-Yu Schive, Tzihong Chiueh, Tom Broadhurst, and Kuan-Wei Huang, "Contrasting Galaxy Formation from Quantum Wave Dark Matter, ψDM, with ΛCDM, using Planck and Hubble Data," Astrophys. J. **818**, 89 (2016),

arXiv:1508.04621 [astro-ph.GA].
[42] P. S. Corasaniti, S. Agarwal, D. J. E. Marsh, and S. Das, "Constraints on dark matter scenarios from measurements of the galaxy luminosity function at high redshifts," Phys. Rev. D **95**, 083512 (2017), arXiv:1611.05892 [astro-ph.CO].
[43] Mona Dentler, David J. E. Marsh, Renée Hložek, Alex Laguë, Keir K. Rogers, and Daniel Grin, "Fuzzy Dark Matter and the Dark Energy Survey Year 1 Data," (2021), arXiv:2111.01199 [astro-ph.CO].
[44] Keir K. Rogers and Hiranya V. Peiris, "Strong Bound on Canonical Ultralight Axion Dark Matter from the Lyman-Alpha Forest," Phys. Rev. Lett. **126**, 071302 (2021), arXiv:2007.12705 [astro-ph.CO].
[45] David J. E. Marsh, "Nonlinear hydrodynamics of axion dark matter: Relative velocity effects and quantum forces," Phys. Rev. D **91**, 123520 (2015), arXiv:1504.00308 [astro-ph.CO].
[46] Neal Dalal, Ue-Li Pen, and Uros Seljak, "Large-scale BAO signatures of the smallest galaxies," J. Cosm. Astropart. Phys. **2010**, 007 (2010), arXiv:1009.4704 [astro-ph.CO].
[47] Julian B. Muñoz, Cora Dvorkin, and Abraham Loeb, "21-cm Fluctuations from Charged Dark Matter," Phys. Rev. Lett. **121**, 121301 (2018), arXiv:1804.01092 [astro-ph.CO].
[48] Steven R. Furlanetto, S. Peng Oh, and Frank H. Briggs, "Cosmology at low frequencies: The 21 cm transition and the high-redshift Universe," Phys. Rep. **433**, 181–301 (2006), arXiv:astro-ph/0608032 [astro-ph].
[49] Anastasia Fialkov, Rennan Barkana, Arazi Pinhas, and Eli Visbal, "Complete history of the observable 21 cm signal from the first stars during the pre-reionization era," Mon. Not. R. Astron. Soc. **437**, L36–L40 (2014), arXiv:1306.2354 [astro-ph.CO].
[50] Abraham Loeb and Matias Zaldarriaga, "Measuring the small - scale power spectrum of cosmic density fluctuations through 21 cm tomography prior to the epoch of structure formation," Phys. Rev. Lett. **92**, 211301 (2004), arXiv:astro-ph/0312134.
[51] S. A. Wouthuysen, "On the excitation mechanism of the 21-cm (radio-frequency) interstellar hydrogen emission line." Astron. J. **57**, 31–32 (1952).
[52] George B. Field, "Excitation of the Hydrogen 21-CM Line," Proceedings of the IRE **46**, 240–250 (1958).
[53] Christopher M. Hirata, "Wouthuysen-Field coupling strength and application to high-redshift 21 cm radiation," Mon. Not. Roy. Astron. Soc. **367**, 259–274 (2006), arXiv:astro-ph/0507102.
[54] Fabio Pacucci, Andrei Mesinger, Stefano Mineo, and Andrea Ferrara, "The X-ray spectra of the first galaxies: 21 cm signatures," Mon. Not. Roy. Astron. Soc. **443**, 678–686 (2014), arXiv:1403.6125 [astro-ph.CO].
[55] Jonathan R. Pritchard and Steven R. Furlanetto, "21 cm fluctuations from inhomogeneous X-ray heating before reionization," Mon. Not. Roy. Astron. Soc. **376**, 1680–1694 (2007), arXiv:astro-ph/0607234.
[56] Miguel F. Morales and J. Stuart B. Wyithe, "Reionization and Cosmology with 21 cm Fluctuations," Ann. Rev. Astron. Astrophys. **48**, 127–171 (2010), arXiv:0910.3010 [astro-ph.CO].
[57] Andrei Mesinger, "Reionization and Cosmic Dawn: theory and simulations," IAU Symp. **333**, 3–11 (2017), arXiv:1801.02649 [astro-ph.CO].
[58] John H. Wise, "Cosmic reionisation," Contemp. Phys. **60**, 145–163 (2019), arXiv:1907.06653 [astro-ph.CO].
[59] A. Loeb and S. Furlanetto, *The First Galaxies in the Universe* (Princeton University Press, 2013).
[60] Y. B. Zel'Dovich, "Gravitational instability: an approximate theory for large density perturbations." Astron. Astrophys. **500**, 13–18 (1970).
[61] Ravi K. Sheth and Giuseppe Tormen, "Large-scale bias and the peak background split," Mon. Not. R. Astron. Soc. **308**, 119–126 (1999), arXiv:astro-ph/9901122 [astro-ph].
[62] Sara Seager, Dimitar D. Sasselov, and Douglas Scott, "RECFAST: Calculate the Recombination History of the Universe," (2011), ascl:1106.026.
[63] Andrei Mesinger, Steven Furlanetto, and Renyue Cen, "21CMFAST: a fast, seminumerical simulation of the high-redshift 21-cm signal," Mon. Not. R. Astron. Soc. **411**, 955–972 (2011), arXiv:1003.3878 [astro-ph.CO].
[64] Steven G. Murray, Bradley Greig, Andrei Mesinger, Julian B. Muñoz, Yuxiang Qin, Jaehong Park, and Catherine A. Watkinson, "21cmFAST v3: A Python-integrated C code for generating 3D realizations of the cosmic 21cm signal," J. Open Source Softw. **5**, 2582 (2020), arXiv:2010.15121 [astro-ph.IM].
[65] Dmitriy Tseliakhovich, Rennan Barkana, and Christopher Hirata, "Suppression and Spatial Variation of Early Galaxies and Minihalos," Mon. Not. Roy. Astron. Soc. **418**, 906 (2011), arXiv:1012.2574 [astro-ph.CO].
[66] Diego Blas, Julien Lesgourgues, and Thomas Tram, "The Cosmic Linear Anisotropy Solving System (CLASS). Part II: Approximation schemes," J. Cosm. Astropart. Phys. **2011**, 034 (2011), arXiv:1104.2933 [astro-ph.CO].
[67] Michael S. Turner, "Coherent Scalar Field Oscillations in an Expanding Universe," Phys. Rev. D **28**, 1243 (1983).
[68] L. F. Abbott and P. Sikivie, "A Cosmological Bound on the Invisible Axion," Phys. Lett. B **120**, 133–136 (1983).
[69] Michael Dine and Willy Fischler, "The Not So Harmless Axion," Phys. Lett. B **120**, 137–141 (1983).
[70] John Preskill, Mark B. Wise, and Frank Wilczek, "Cosmology of the Invisible Axion," Phys. Lett. B **120**, 127–132 (1983).
[71] Wayne Hu, "Structure formation with generalized dark matter," Astrophys. J. **506**, 485–494 (1998), arXiv:astro-ph/9801234.
[72] Wayne Hu, Rennan Barkana, and Andrei Gruzinov, "Cold and fuzzy dark matter," Phys. Rev. Lett. **85**, 1158–1161 (2000), arXiv:astro-ph/0003365.
[73] Jai-chan Hwang and Hyerim Noh, "Axion as a Cold Dark Matter candidate," Phys. Lett. B **680**, 1–3 (2009), arXiv:0902.4738 [astro-ph.CO].
[74] Hsi-Yu Schive, Tzihong Chiueh, and Tom Broadhurst, "Cosmic Structure as the Quantum Interference of a Coherent Dark Wave," Nature Phys. **10**, 496–499 (2014), arXiv:1406.6586 [astro-ph.GA].
[75] Jan Veltmaat and Jens C. Niemeyer, "Cosmological particle-in-cell simulations with ultralight axion dark matter," Phys. Rev. D **94**, 123523 (2016), arXiv:1608.00802 [astro-ph.CO].
[76] Adrian Liu, Aaron R. Parsons, and Cathryn M. Trott, "Epoch of reionization window. I. Mathematical formalism," Phys. Rev. D **90**, 023018 (2014), arXiv:1404.2596 [astro-ph.CO].

[77] Adrian Liu, Aaron R. Parsons, and Cathryn M. Trott, "Epoch of reionization window. II. Statistical methods for foreground wedge reduction," Phys. Rev. D **90**, 023019 (2014), arXiv:1404.4372 [astro-ph.CO].

[78] Jonathan C. Pober, Aaron R. Parsons, David R. DeBoer, Patrick McDonald, Matthew McQuinn, *et al.*, "The Baryon Acoustic Oscillation Broadband and Broad-beam Array: Design Overview and Sensitivity Forecasts," Astron. J. **145**, 65 (2013), arXiv:1210.2413 [astro-ph.CO].

[79] Jonathan C. Pober *et al.*, "What Next-Generation 21 cm Power Spectrum Measurements Can Teach Us About the Epoch of Reionization," Astrophys. J. **782**, 66 (2014), arXiv:1310.7031 [astro-ph.CO].

[80] Jonathan Pober, "21cmSense: Calculating the sensitivity of 21cm experiments to the EoR power spectrum," (2016), ascl:1609.013.

[81] Aaron R. Parsons, Adrian Liu, *et al.*, "New Limits on 21 cm Epoch of Reionization from PAPER-32 Consistent with an X-Ray Heated Intergalactic Medium at $z = 7.7$," Astrophys. J. **788**, 106 (2014), arXiv:1304.4991 [astro-ph.CO].

[82] Joshua S. Dillon and Aaron R. Parsons, "Redundant Array Configurations for 21 cm Cosmology," Astrophys. J. **826**, 181 (2016), arXiv:1602.06259 [astro-ph.IM].

[83] A. P. Beardsley, M. F. Morales, A. Lidz, M. Malloy, and P. M. Sutter, "Adding Context to James Webb Space Telescope Surveys with Current and Future 21 cm Radio Observations," Astrophys. J. **800**, 128 (2015), arXiv:1410.5427 [astro-ph.CO].

[84] Anastasia Fialkov, Rennan Barkana, Eli Visbal, Dmitriy Tseliakhovich, and Christopher M. Hirata, "The 21-cm signature of the first stars during the Lyman-Werner feedback era," Mon. Not. R. Astron. Soc. **432**, 2909–2916 (2013), arXiv:1212.0513 [astro-ph.CO].

[85] Eli Visbal, Zoltán Haiman, Bryan Terrazas, Greg L. Bryan, and Rennan Barkana, "High-redshift star formation in a time-dependent Lyman–Werner background," Mon. Not. Roy. Astron. Soc. **445**, 107–114 (2014), arXiv:1402.0882 [astro-ph.CO].

[86] Marie E. Machacek, Greg L. Bryan, and Tom Abel, "Simulations of pregalactic structure formation with radiative feedback," Astrophys. J. **548**, 509 (2001), arXiv:astro-ph/0007198.

[87] John H. Wise and Tom Abel, "Resolving the Formation of Protogalaxies. 3. Feedback from the First Stars," Astrophys. J. **685**, 40 (2008), arXiv:0710.3160 [astro-ph].

[88] Asimina Arvanitaki and Sergei Dubovsky, "Exploring the String Axiverse with Precision Black Hole Physics," Phys. Rev. D **83**, 044026 (2011), arXiv:1004.3558 [hep-th].

[89] David J. E. Marsh and Jens C. Niemeyer, "Strong Constraints on Fuzzy Dark Matter from Ultrafaint Dwarf Galaxy Eridanus II," Phys. Rev. Lett. **123**, 051103 (2019), arXiv:1810.08543 [astro-ph.CO].

[90] Matthew J. Stott and David J. E. Marsh, "Black hole spin constraints on the mass spectrum and number of axionlike fields," Phys. Rev. D **98**, 083006 (2018), arXiv:1805.02016 [hep-ph].

[91] Daniel Grin, Mustafa A. Amin, Vera Gluscevic, Renée Hlŏzek, David J. E. Marsh, Vivian Poulin, Chanda Prescod-Weinstein, and Tristan L. Smith, "Gravitational probes of ultra-light axions," (2019), arXiv:1904.09003 [astro-ph.CO].